JMEPEG (2000) 9:477-488

Carbide and Hardness Development in the Heat-Affected Zone of Tempered and Postweld Heat-Treated 2.25Cr-1Mo Steel Weldments

B.E. Peddle and C.A. Pickles

(Submitted 18 November 1998; in revised form 1 June 2000)

The temper-bead and the conventional weaving, multipass welding procedures have been developed to eliminate postweld heat treatment (PWHT) of creep resistant 2.25Cr-1Mo steel. Both procedures aim to refine and temper the heat-affected zone (HAZ). The temper-bead procedure resulted in a martensitic HAZ and a homogeneous fine-grain size. Hardness was not decreased by high heat input weaving fillout passes. Upper bainite developed in the conventional weaving HAZ, although grain refinement was inhomogeneous and some martensite was present. However, the conventional weaving procedure appears to produce a lower as-welded hardness than the temper-bead procedure.

The carbides within the temper-bead HAZ aged more rapidly than those in the conventional weaving HAZ as a result of the initial martensitic temper-bead HAZ microstructure. Previous work indicated that the temper-bead HAZ toughness decreased after 1000 h of tempering at 538 °C. This correlated with the coarsening and the agglomeration of the carbides.

The maximum hardness occurred within the as-welded coarse-grained HAZ. The PWHT resulted in the greatest decrease in hardness and also reduced hardness variability throughout the HAZ. The hardness decreased to postweld heat-treated values after approximately 1000 h at 538 °C and softening was associated with the precipitation and coarsening of acicular carbides and the development of coarse grain-boundary carbides.

Keywords 2.25 Cr-1.0Mo steel, heat-affected zone, postweld heat treatment, microstructure, welding

1. Introduction

Chromium-molybdenum steels are employed extensively for heavy section low alloy steel structural and pressure boundary components in thermal power generating stations.[1,2] In particular, 2.25Cr-1Mo steels are often employed for operating temperatures in the range of 371 to 540 °C.[3,4] When repairing these components, it is often necessary to perform a high-temperature postweld heat treatment (PWHT). However, this procedure can be expensive, as it requires extended down time. The elimination of the PWHT for these repairs could result in significant time and cost savings.

One possible solution to this problem is to return the low alloy repair heat-affected zone (HAZ) to service and operate at a high temperature (*i.e.*, a typical plant operating temperature of 538 °C). In this way, the weld repair will be heat treated *in situ*. Clearly, it is necessary to understand the effects of the welding process and any subsequent heat treatment on the microstructure of the material.

During welding, the base metal is subjected to severe thermal cycling. This results in significant alteration of the original microstructure in a localized region adjacent to the fusion line. This region is known as the heat-affected zone (HAZ). The microstructure of the HAZ is inhomogeneous and can be divided into the coarse-grain HAZ (CGHAZ), the fine-grain HAZ (FGHAZ), the intercritical HAZ (ICHAZ), and the subcritical HAZ (SCHAZ). The peak temperatures are higher near the fusion line and decrease rapidly toward the base metal so that the microstructure developed within each zone is a direct result of the thermal history of that location.

For a given material composition, the peak temperature reached during heating and the cooling rate are the two most important factors that affect the microstructural development in the HAZ. The important temperatures for steel are the A_{c3} and A_{cl} temperatures. For a 2.25Cr-1Mo-0.14C steel, A_{c3} is approximately 894 °C and A_{cl} is 780 °C.[5] Above A_{c3}, the microstructure is fully austenitic. The solubility of carbides is greatly increased at these temperatures and the temperature, which divides restricted and unrestricted austenitic grain growth, is determined by the grain-refining strength of the carbides.[6] In a 2.25Cr-1Mo steel, the carbides fully dissolve between 1000 and 1050 °C, leading to unrestricted austenitic grain growth above this temperature range.[1,7–9]

The microstructure that develops in the HAZ of a 2.25Cr-1Mo steel has been previously described in the literature.[10,11,12] It was found that the conventional weaving procedure resulted in the development of a predominantly tempered bainitic CGHAZ and FGHAZ. The temper-bead procedure produced a fine-grained martensitic structure within the same zones.

The cooling rate strongly affects the type of microstructure that develops where transformation to austenite has occurred.[5,7,11] It is usually expressed as the cooling time between 800 and 500 °C, that is, $t_{800–500}$ (s). Low cooling rates promote transformation at higher temperatures, leading to the

B.E. Peddle and **C.A. Pickles**, Department of Materials and Metallurgical Engineering, Queen's University, Kingston, ON, Canada K7L 3N6.

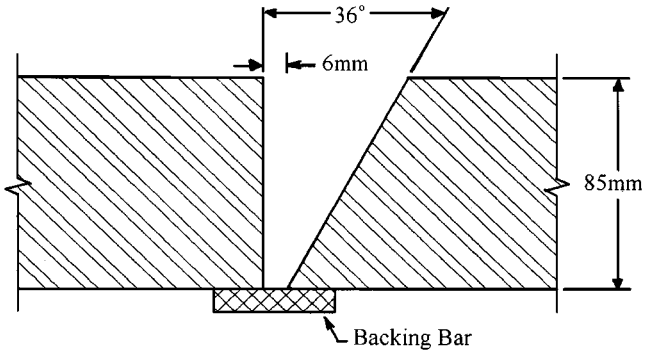

Fig. 1 Schematic diagram of the joint preparation for each welding procedure[15]

Table 1 Pipe dimensions

Length	Outside diameter	Thickness
610 mm	406 mm	82 mm

Table 2 Chemical analysis of base metal

Element	C	Mn	Cr	Mo	Si	P	S
Mass percent	0.11	0.39	2.06	0.92	0.34	0.011	0.013

development of low-hardness transformation products such as ferrite, pearlite, or upper bainite. High cooling rates result in martensite or lower bainite, which develop at lower temperatures, and are high-hardness transformation products. Usually, a mixed microstructure develops within the HAZ so that it is not homogeneous, and the mechanical properties may vary from zone to zone.[13]

In the present research, both the conventional weaving and the temper-bead welding procedures were employed. As-welded samples, without PWHT, were tempered up to 4000 h at a simulated operating temperature of 538 °C and these were compared to control samples that had been subjected to a simulated PWHT at 725 °C for 3 h, which is in accord with the ASME Boiler and Pressure Vessel Code.[14] The changes in the microstructure and the carbide morphology and their compositions were related to the mechanical properties of the material.

2. Experimental Procedures

2.1 Material

The steel employed was a ferritic 2.25Cr-1Mo (SA335-P22) seamless steel pipe. The dimensions of the pipe are shown in Table 1 and the manufacturer-supplied chemical analysis is shown in Table 2.

2.2 Weld Preparation

The pipe was received in the normalized and tempered condition. For both the temper-bead weld and the conventional weaving weld, a 36° single-bevel joint was prepared and a backing bar was employed, as shown in Fig. 1. The use of a backing bar and a bevel joint is not standard practice, but was necessary to ensure that the dimensions of the HAZ were relatively uniform.

Table 3 Conventional weaving procedure[15]

Welding parameters	Value
Preheat temperature (minimum)	232°C
Postheat temperature	232 °C
Interpass temperature (maximum)	288 °C
Filler metal	E9018B3
Joint preparation	Machine or mechanically ground
First layer electrodes	N/A
Second layer electrodes	N/A
Fillout electrodes	3/32 in., 1/8 in., and 5/32 in., weave
Voltage (V)	3/32 in.—20 to 24 1/8 in.—21 to 24 5/32 in.—22 to 25
Current (A)	3/32 in.— 80 to 130 1/8 in.—100 to 160 5/32 in.—130 to 2200
Travel speed (mm/min)	3/32 in.—180 to 400 1/8 in.—180 to 400 5/32 in.—180 to 400
Heat input (J/mm)	240 to 1040 315 to 1280 429 to 1667
Non-destructive testing	Magnetic particle inspection, radiographic inspection

The conventional weaving weld parameters are given in Table 3. The joint was fabricated in the 1G position. The temper-bead weld parameters are listed in Table 4. The stringer beads were deposited on the vertical face of the joint in the flat position prior to tacking the two pipe sections together and the weaving fillout passes were made with the joint in the 1G position. Preheat was maintained for 2 h following the completion of welding to permit hydrogen diffusion. After cooling to room temperature, the weldments were subjected to nondestructive testing by magnetic-particle inspection and radiography. Schematic diagrams of each joint are shown in Fig. 2.

2.3 Heat Treatment

Each weldment was sectioned into eight samples, the dimensions of which were approximately 76 × 76 × 305 mm. Several sections from each weld were left in the as-welded condition. The remainder were heat treated in a high-temperature resistance furnace in an air atmosphere, either at a temperature of 538 ± 5 °C for times of 100, 1000, 2000, and 4000 h in order to simulate exposure to service temperature or at a temperature of 725 ± 5 °C for 3 h to simulate PWHT. Sectioning of the joint and heat treatment were performed in a previous study[15].

Smaller sections, approximately 10 × 20 mm were cut from the heat-treated sections such that several weld beads were encompassed. Each sample was taken from the mid-section of

Table 4 Temper-bead welding procedure[15]

Welding parameter	Value
Preheat temperature (minimum)	232 °C
Postheat temperature	232 °C
Interpass temperature (maximum)	288 °C
Filler metal	E9018B3
Joint preparation	Machine or mechanically ground
First layer electrodes	3/32 in., 50% overlap, stringer bead
Second layer electrodes	1/8 in., 50% overlap, stringer bead
Fillout electrodes	5/32 in., weave
Voltage (V)	3/32 in.—21 1/8 in.—22 5/32 in.—23
Current (A)	3/32 in.—80 1/8 in.—120 5/32 in.—170
Travel speed (mm/min)	3/32 in.—296 1/8 in.—332 5/32 in.—240
Heat input (J/mm)	340 496 978
Non-destructive testing	Magnetic particle inspection, radiographic inspection

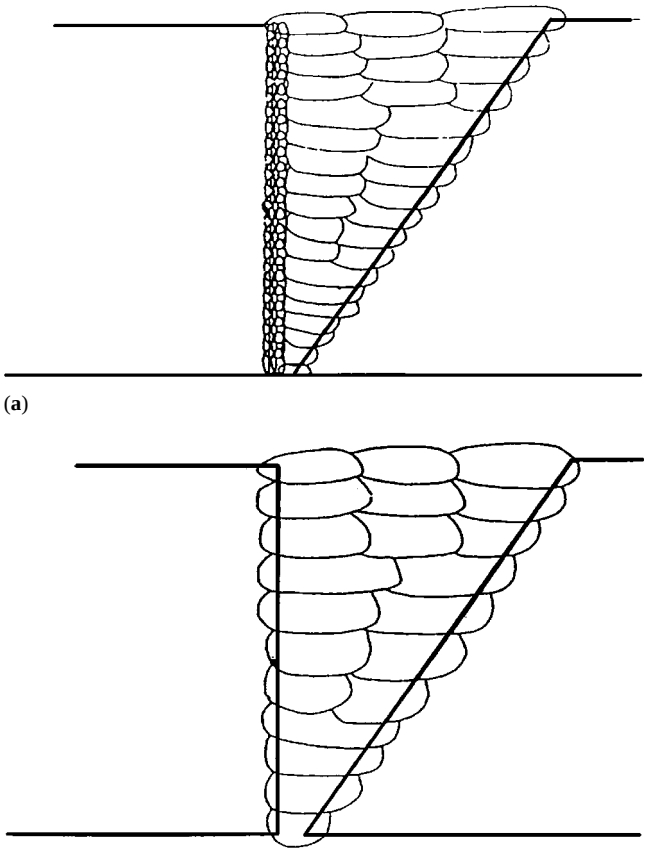

Fig. 2 Schematic diagram of the placement of the weld beads in: (**a**) the temper beadtemper-bead weld, and (**b**) the conventional weaving weld[15]

the flat face of the joint and was oriented transverse to the welding direction and normal to the pipe surface. These sections were used for microhardness testing and the preparation of carbon extraction replicas.

2.4 Microhardness Testing

Vickers microhardness testing was performed on each weld sample. Hardness traverses were made at the bay region and at the root of a weld bead, such that the traverse was perpendicular to the fusion line, spanning a portion of the weld metal, the HAZ, and a portion of the unaffected base metal, as shown in Fig. 3. The bay region is the intersection point of two weld beads.

Samples were mounted in bakelite and successively ground on 120, 240, 400, and 600 grit SiC paper. The surface was rough polished with 6 μm diamond paste and finished with a 1 μm alumina slurry. To eliminate polishing artifacts and scratches, the samples were lightly etched in 2% Nital and repolished with 1 μm alumina. They were again etched with 2% Nital until the microstructure of the weld HAZ was clearly delineated.

Indentations were made with a Leitz microhardness tester using a 400 g load applied for 15 s. An indentation was first made at the fusion line and the positions of subsequent indentations were measured relative to it. The spacing between the center points of adjacent indentations was a minimum of twice the average indentation diagonal length. Indentation diagonals were measured at a magnification of 500× using an image analyzer and a program that measured linear distance. Microhardness values were determined using the following equation:[16]

$$HV = \frac{1854.4P}{D^2}$$

where P is the applied load (grams) and D is the average length (μm) of the two indentation diagonals.

Each microhardness traverse was repeated after grinding to remove the previous hardness traverse. The surface was prepared as described previously. Traverses were repeated three times and an average hardness value for each position in the HAZ was determined.

2.5 Transmission Electron Microscope Studies

For each welding procedure, carbon extraction replicas spanning the HAZ were taken from the root region of a weld-bead deposit. The replicas were taken from regions that exhibited similar microstructural refinement to minimize variation between samples. Extraction replicas were also prepared from the unaffected base metal several centimeters away from the HAZ.

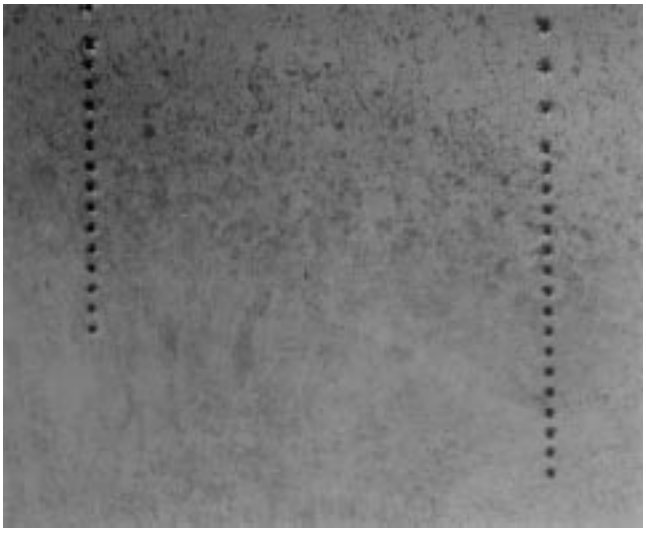

(**a**)

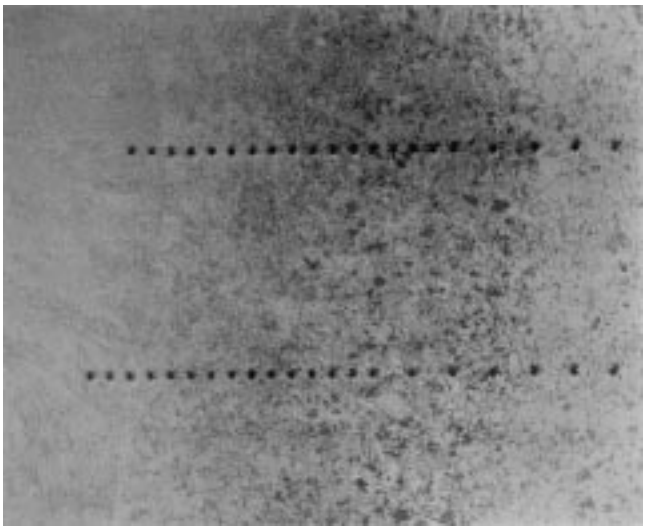

(**b**)

Fig. 3 Location of the microhardness traverses at the root and bay regions of a weld bead within the HAZ of: (**a**) the temper bead weld (×31), and (**b**) the conventional weaving weld (×31)

Samples were successively ground on 120, 240, 400, and 600 grit SiC paper. The surface was rough polished with 6 μm diamond paste and then finished with a 1 μm alumina slurry. Polishing artifacts and scratches were removed by lightly etching in 2% Nital and repolishing with 1 μm alumina.

The sample was etched with 2% Nital until the microstructure of the HAZ was well-defined. A number of microhardness indentations were then made along the fusion line and perpendicular to it to facilitate rapid identification of the fusion line on the replica. The sample was then carbon coated until the coating color was blue-brown. Under a stereomicroscope, at a magnification of approximately 60×, individual weld metal beads, the fusion line, and the HAZ were clearly delineated. Sections approximately 2 mm square were scribed into the carbon film. A single replica was sufficient to span the entire HAZ of the temper-bead weld. The area from the fusion line to the ICHAZ of the conventional weaving weld was covered by one replica, which was sufficient for the purpose of analysis.

The carbon extraction replicas were removed by anodic dissolution of the metal substrate. Samples were immersed in a 4% HCl-96% methanol solution at room temperature. Fresh electrolyte was used for each sample. The voltage was varied between 3 and 10 V DC, giving a current ranging from 0.075 to 0.1 A, for up to 30 min. After the extraction replicas had separated from the metal, they were rinsed in distilled water containing methanol. Subsequently, they were floated on distilled water and mounted on 3 mm diameter 200-mesh copper grids for analysis. Microhardness indentations on the extraction replica were visible under a stereomicroscope and it was possible, by trial and error, to align the fusion line indentations parallel to a copper grid bar. The copper grid bars divided the sample into 125 μm areas in which transmission electron microscope (TEM)/energy dispersive spectroscopy (EDS) analysis was performed.

A Philips (Philips Electronic Instruments Corp., Mahwah, NJ) CM20 scanning TEM equipped with EDS was operated in the TEM mode to obtain electron diffraction patterns and x-ray spectra from the various precipitates present on the carbon extraction replicas. The microscope accelerating voltage was 200 keV and for EDS, the condenser aperture size was 100 μm, the spot size was varied between 27.5 nm and 15 nm depending on the precipitate size, and the sample was inclined at 30° to the beam, giving a take-off angle of 46.19°. Live time was set at 100 s and dead time was set to 25 $\pm$ 5% by adjusting the spot size. To positively identify a carbide, selected area diffraction was first used to obtain an x-ray spectrum. Carbides were also identified by comparison of the x-ray spectra with those in the literature.[17–23]

3. Results and Discussion

3.1 Metallography-Base Metal and Weldments

The microstructure of the base metal was ferrite and pearlite. Pearlitic clusters and grain-boundary carbides were identified as $M_{23}C_6$. Within the ferrite grains, carbides were identified as cuboidal $M_{23}C_6$ and acicular M_2C. Minor amounts of M_7C_3 were also present within the matrix. The TEM micrographs of the carbides are shown in Fig. 4.

The conventional weaving HAZ consisted of upper bainite and some martensite. Some grain refinement occurred, but it was inhomogeneous. The grain size was relatively large as a result of the relatively high heat input that was used to deposit the weaved beads. The temper-bead procedure was effective in refining the CGHAZ and the fine-grained austenite transformed into martensite.

3.2 Microhardness Testing

The average microhardness values of the root and bay regions of the conventional weaving HAZ are plotted in Fig. 5 and 6. Those for the temper-bead HAZ are shown in Fig. 7 and 8. The temper-bead HAZ and the conventional weaving HAZ were similar in many respects. The maximum hardness values occurred within the as-welded CGHAZ and the hardness

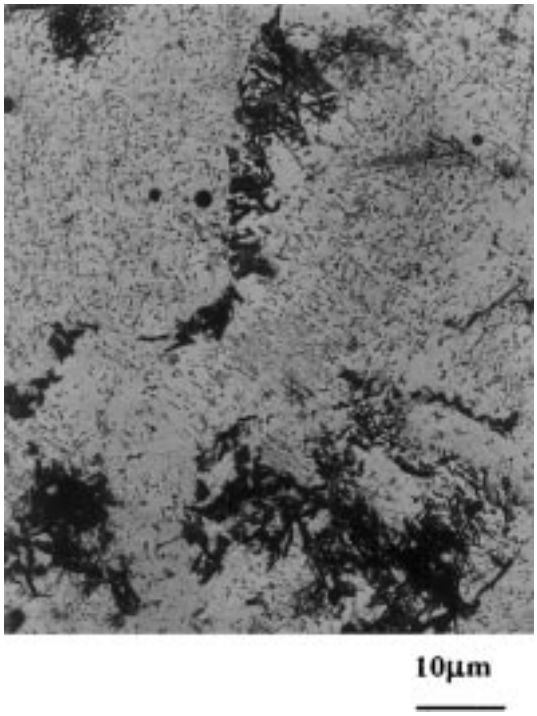

(**a**)

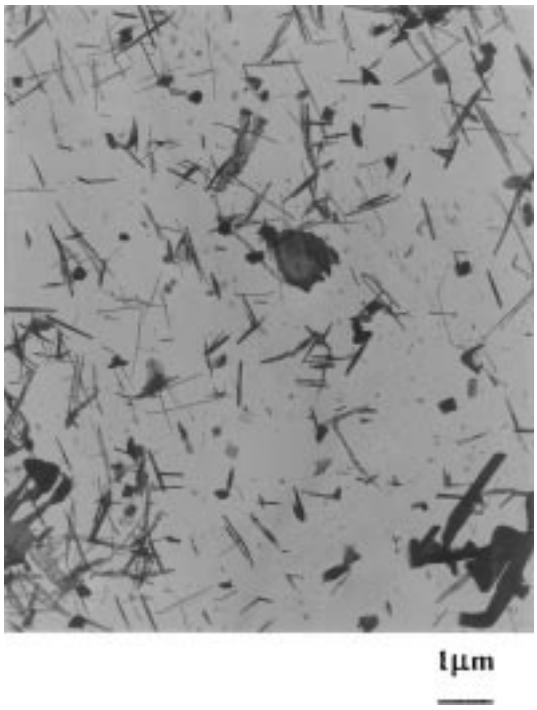

(**b**)

Fig. 4 (**a**) TEM micrograph of the base metal showing clusters of pearlitic $M_{23}C_6$ and dense precipitation of acicular M_2C within ferrite grains (×1.2k),) and (**b**) acicular M_2C and cuboidal $M_{23}C_6$ precipitates within a ferrite grain (×6.61k)

decreased with increasing distance from the fusion line until a constant value of approximately 160 HV was reached in the base metal. In the as-welded condition, the maximum hardness in the temper-bead CGHAZ was found to be approximately 400 HV, while the maximum hardness found in the CGHAZ of the conventional weaving weld was significantly lower, approximately 305 HV.

As can be seen in Fig. 5, the conventional weaving weld sample tempered for 100 h at 538°C is much harder than the sample in the as-welded condition. The microstructure observed in the CGHAZ of the 100 h sample was coarse grained, tempered martensite, whereas that of the as-welded CGHAZ was upper bainite. This illustrates the significant microstructural variability that can develop in the HAZ of a weldment made by the conventional weaving procedure that is not strictly controlled and permits large variation in heat input. Hence, in some regions, the maximum as-welded hardness of the conventional weaving CGHAZ could approach that of the as-welded temper-bead CGHAZ, that is, approximately 400 HV.

The simulated PWHT at 725 °C for 3 h resulted in the greatest decrease in hardness, approximately 100 HV for the conventional weaving weld and as much as 190 HV in the case of the temper-bead weld. The PWHT also significantly reduced hardness variability throughout the HAZ. Exposure to an operating temperature of 538 °C produced the largest decrease in hardness within the first 100 h of tempering. After an exposure time of 500 h, the rate of softening decreased drastically, and hardness values similar to those of the PWHT HAZ were attained at tempering times between 1000 and 4000 h. In all cases, the bay was softer than the root after identical tempering times and followed the same softening trend during heat treatment.

3.3 Comparison of Welding Techniques

Microhardness results showed that the hardness within the CGHAZ and the FGHAZ of the temper-bead weld decreased very rapidly, dropping by as much as 140 HV within the first 500 h of tempering at 538 °C (Fig. 7). The rate of softening slowed drastically after this period, and the hardness at 1000 and 4000 h had decreased only slightly below that at 500 h. The conventional weaving HAZ hardness was similar to that of the temper-bead HAZ after tempering for 500 h, and, neglecting the 100 h hardness traverse, the hardness decreased at a much lower rate, and dropped by approximately 60 HV (Fig. 5).

The tempering behaviors of martensite and bainite are quite different, as illustrated by the initial high rate of softening observed in the martensitic temper-bead HAZ. During tempering, martensite forms a dispersion of very fine carbides due to the saturation of the matrix with respect to carbon.[24] The fine carbides coarsen rapidly, and this leads to the initial drastic decrease in hardness observed in the temper-bead HAZ. Upper bainite tempers differently because M_3C precipitates during the austenite-to-bainite transformation. This decreases the concentration of carbon dissolved in the matrix, which lowers the driving force for further carbide precipitation, and, since the carbides that form during transformation are relatively large, they coarsen slowly.[24] As a result, the initial hardness of the conventional weaving HAZ decreased at a much slower rate.

The heat treatment temperature strongly affects the diffusion rates of Cr and Mo. Consequently, temperature has a very strong influence on the coarsening behavior of the carbides, as shown

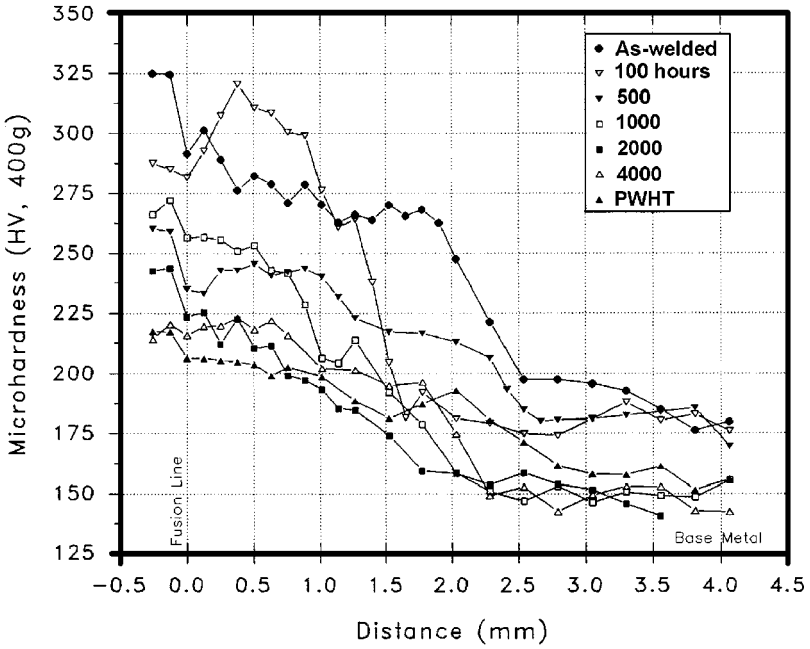

Fig. 5 Microhardness traverses of the root region of the conventional weaving HAZ

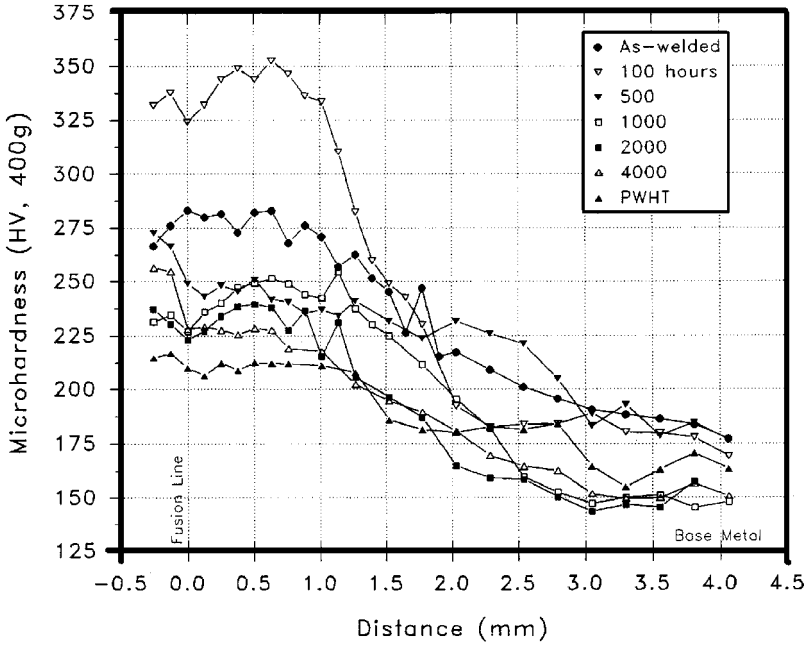

Fig. 6 Microhardness traverses of the bay region of the conventional weaving HAZ

in Fig. 9 and 10, and the type of carbide that precipitates, since both are dependent on the diffusion of carbide-forming elements. Although not strictly applicable, because of the thermal history of the HAZ and the differing alloy contents of the two steels, it would be expected that higher temperatures, such as the PWHT temperature (725 °C), would favor the rapid development of the higher alloy carbides, such as $M_{23}C_6$, whereas extended exposure at the service temperature promotes slow progression through the carbide evolution sequence.[25] The diffusion rates of Mo and Cr are significantly lower at 538 °C and the thermal energy required for the rapid nucleation of the higher alloy, equilibrium carbides is not available. As a result, acicular M_2C remains coherent with the matrix and resists coarsening and dissolution, whereas M_3C, which is unstable, transforms completely to M_7C_3, which, in turn, is slowly replaced by M_6C.

Within the first 100 h of tempering, precipitation of very fine, intragranular M_2C was observed in the temper-bead HAZ,

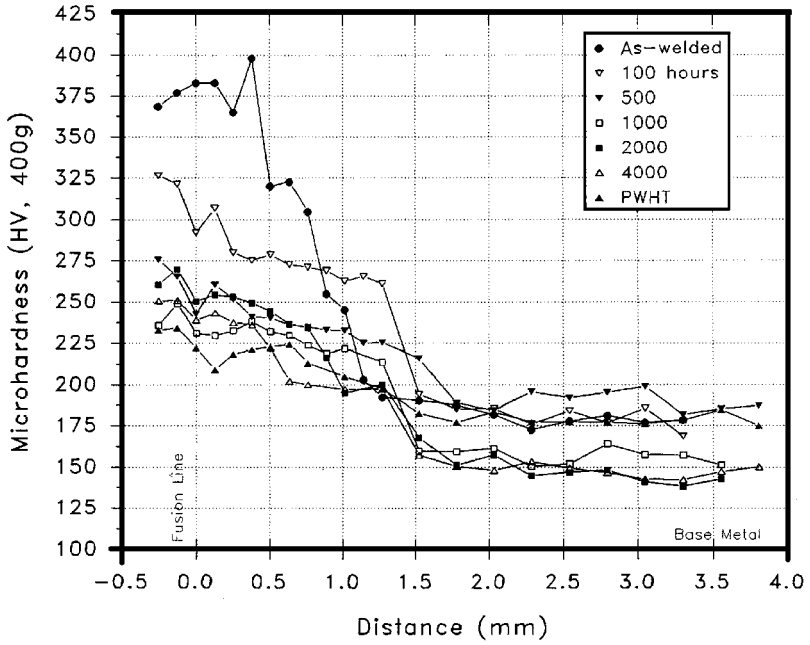

Fig. 7 Microhardness traverses of the root region of the temper bead-HAZ

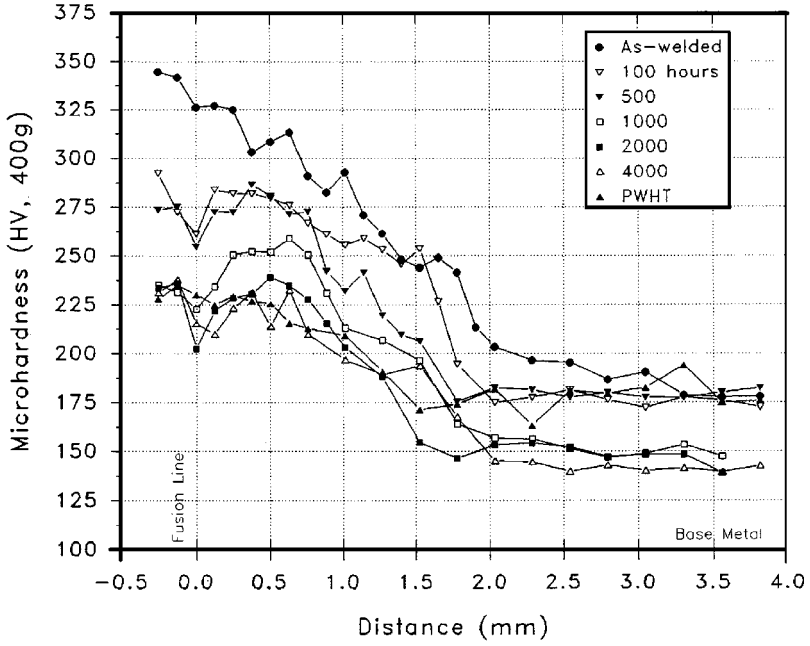

Fig. 8 Microhardness traverses of the bay region of the temper bead-HAZ

in addition to increased precipitation of M_3C. Figure 9(c) illustrates the high density of fine, acicular M_2C carbides and larger M_3C carbides at lath boundaries and grain boundaries within the CGHAZ. This correlates with the initial high rate of hardness reduction within the temper-bead HAZ, as presented in Fig. 7 and 8. The density of acicular M_2C precipitated within ferrite laths continued to increase with tempering time, until between 500 h and 1000 h, as shown by Fig. 9(a) to (h). However, aging of the M_2C and the coarsening and dissolution of M_3C, followed by the precipitation of higher alloy carbides, such as M_7C_3 at grain boundaries, appears to be the primary mode of hardness reduction and corresponds to a greatly reduced rate of softening (Fig. 5 through 8).

The effect of carbide coarsening on the rate of hardness reduction is illustrated by comparison of the 1000 and 4000 h microhardness traverses and comparison of the 1000 h micrographs (Fig. 9e, f and 10e, f) to the 4000 h micrographs (Fig. 9g, h and 10g, h). The grain boundary carbides have coarsened

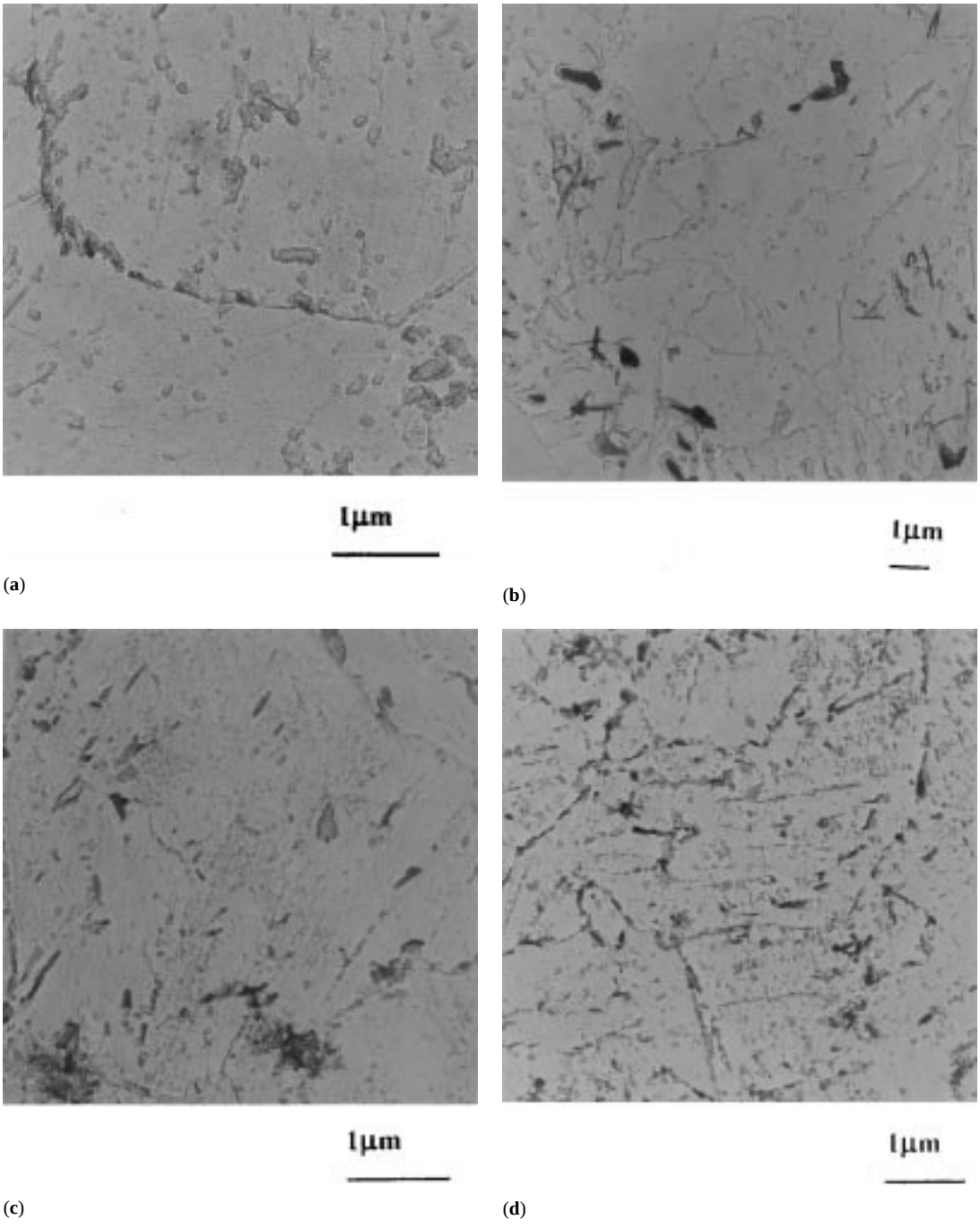

Fig. 9 Development of carbides in the temper-bead HAZ. (**a**) M_3C precipitates at a prior austenite grain boundary within the as-welded CGHAZ (×15.0k); (**b**) partially dissolved M_2C and $M_{23}C_6$ carbides near the ICHAZ/FGHAZ interface (×6.61k); (**c**) intragranular precipitation of fine M_2C, in addition to M_3C, within the CGHAZ after tempering for 100 hours (×15.0k); (**d**) increased precipitation of acicular M_2C within the CGHAZ after tempering for 500 hours (×11.5k) (continued on next page)

significantly between 1000 and 4000 h, although the hardness decreased very little over the same time period. Softening is retarded by acicular M_2C because it remains coherent with the matrix for extended tempering times.[25,26,27] It can be seen in the TEM micrographs (Fig 9c through e) that the matrix M_2C has coarsened to some extent by 4000 h, although this carbide has aged very slowly compared to the grain-boundary carbides.

The microhardness of the HAZ of each weldment approached the values achieved by PWHT after tempering at 538 °C for times between 1000 and 4000 h (Fig. 5 through 8). However, the carbide morphologies were significantly different. The PWHT temperatures favored the rapid development of coarse carbides and the spheroidization and dissolution of fine, acicular precipitates. Comparison of Fig. 9 and 10 shows that

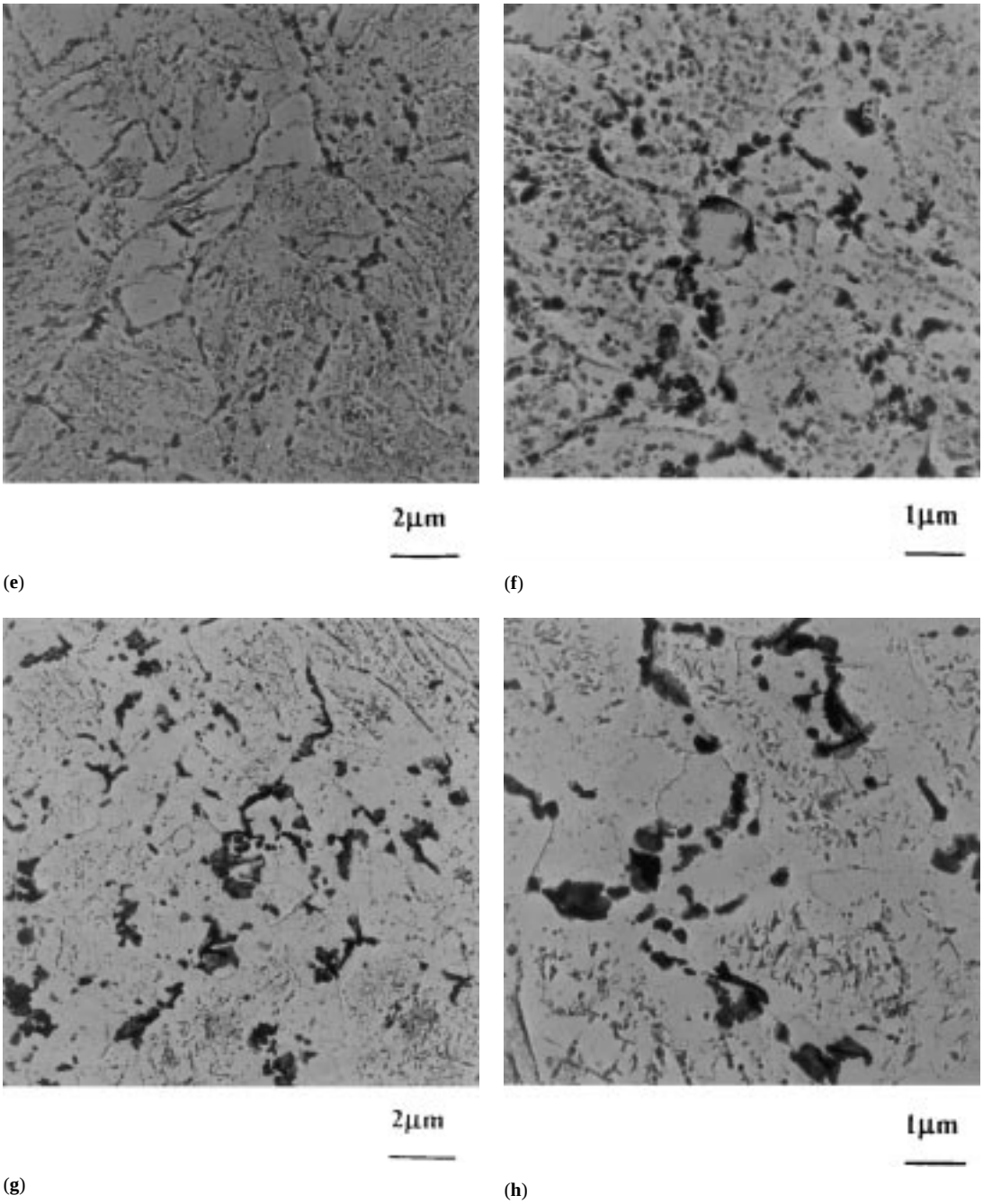

Fig. 9 cont. Development of carbides in the temper-bead HAZ. (**e**) CGHAZ after tempering for 1000 hours showing intense precipitation of M_2C as well as development of grain-boundary carbides (×5.0k); (**f**) enlargement of (e), showing very fine, acicular M_2C and larger grain-boundary carbides (×8.8k); (**g**) CGHAZ after tempering for 4000 hours showing development of irregularly shaped, coarse grain-boundary carbides (×5.0k); and, (**h**) Enlargement of (g), showing acicular M_2C carbides in addition to coarse grain-boundary carbides (×8.8k)

the HAZ tempered at 538 °C, particularly the conventional weaving HAZ, aged much less and retained a high density of fine, acicular M_2C carbides.

Previous work[15] has shown that the room-temperature impact toughness of the temper-bead HAZ decreased substantially after tempering at 538 °C for 1000 h. These results are reproduced in Fig. 11, and it is evident that by 4000 h, the toughness had decreased by approximately 15%, from 210 to 175 J. The observed decrease in toughness was caused by the combination of a small prior austenite grain size, increased grain-boundary precipitation, and large grain-boundary carbides.[25]

Figures 9(e) through (h) are TEM micrographs of the CGHAZ after 1000 and 4000 h. It can readily be seen that the number of grain-boundary carbides increased, and that these carbides coarsened extensively between 1000 and

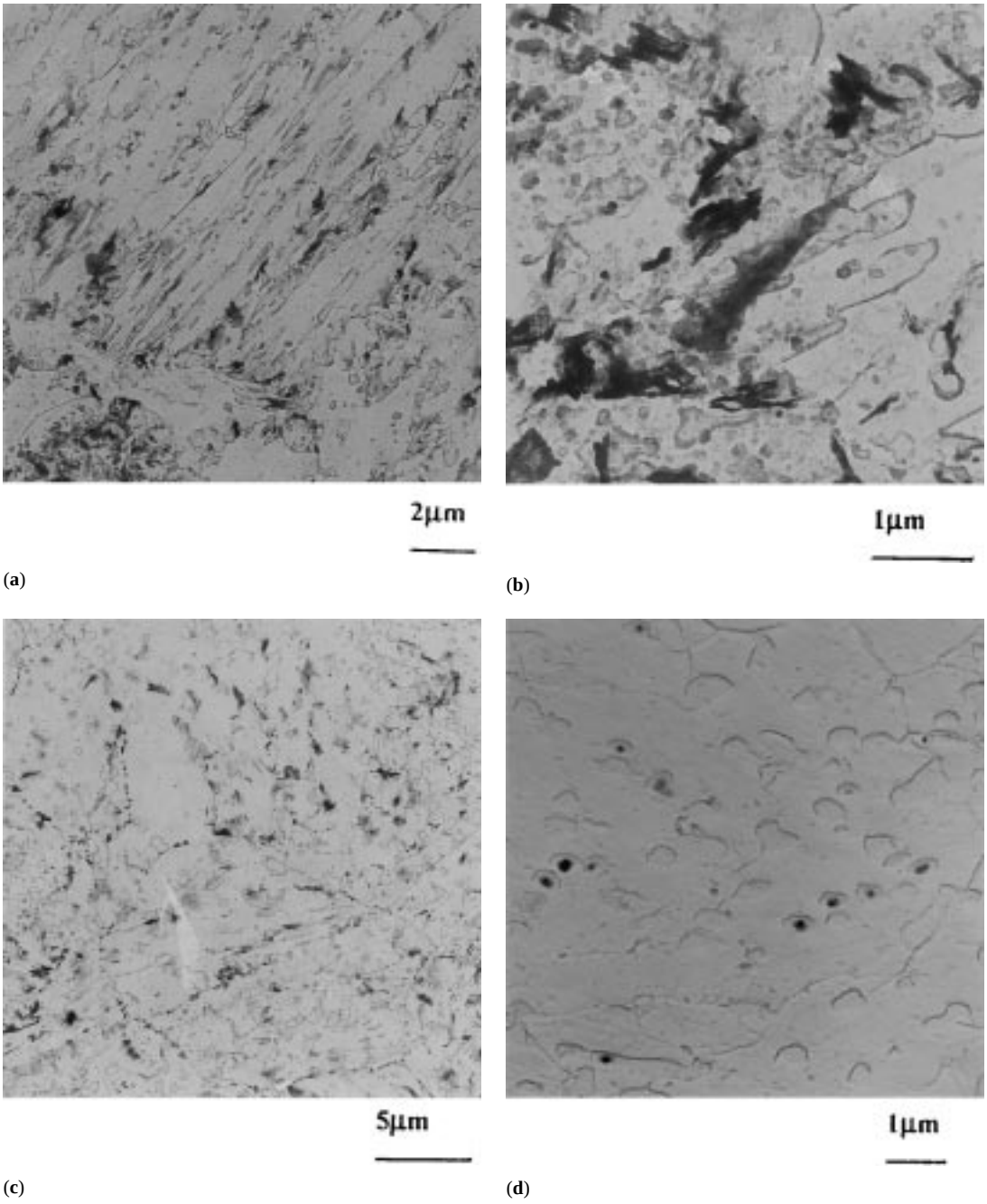

Fig. 10 Development of carbides in the conventional weaving HAZ. (**a**) Upper bainite in the as-welded CGHAZ showing carbide precipitation parallel to lath boundaries (×3.8k); (**b**) enlargement of the area in (a) showing clustering of M_3C precipitates at lath boundaries (×15.0k); (**c**) upper bainite within the FGHAZ showing heavily spheroidized carbides identified as M_6C and M_3C at lath and prior austenite grain boundaries (×2.75k); (**d**) Region near the FGHAZ/ICHAZ interface showing M_6C carbides that had transformed *in situ* from M_2C (×8.8k) (continued on next page)

4000 h. Many of the very large carbides were found to be an agglomeration of M_7C_3 and M_6C carbides, which indicates that the M_7C_3-to-M_6C transformation occurs *in situ*, as reported previously.[25]

Generally, the carbide morphology was irregular and elongated so that the ratio of carbide surface area to grain-boundary surface area increased. In Fig. 9(g), it can be seen that some carbides had agglomerated to the extent that the entire grain boundary was covered. It is probable that this had a detrimental effect on the impact toughness, since a propagating crack could follow a semicontinuous path of low resistance along grain boundaries decorated with large carbides. The observed loss of fracture resistance as a consequence of the coarsening and agglomeration of grain-boundary carbides has been reported

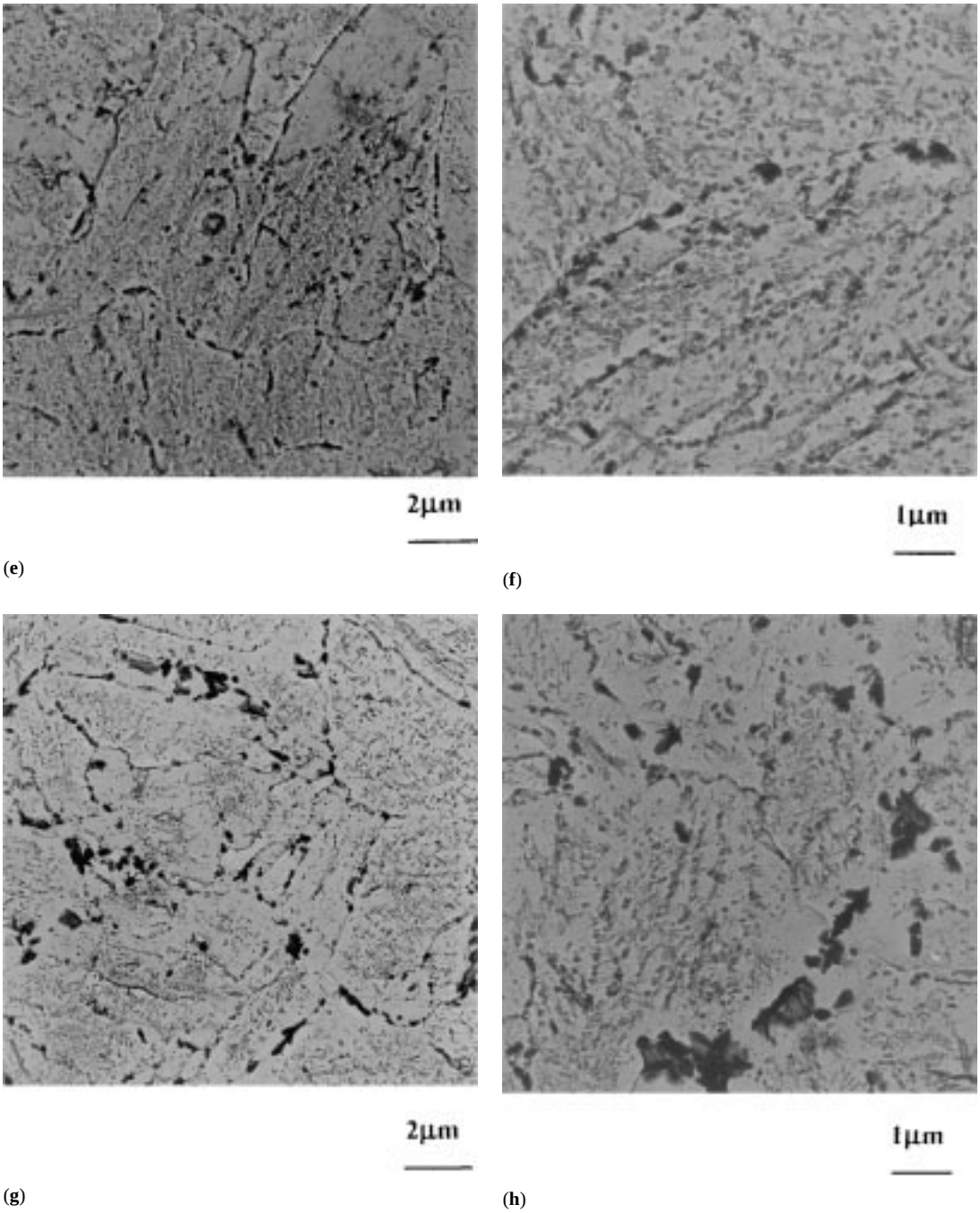

Fig. 10 cont. Development of carbides in the conventional weaving HAZ. (**e**) CGHAZ after tempering for 1000 hours illustrating intense precipitation of intragranular M_2C and development of grain-boundary carbides (×5.0k); (**f**) enlargement of the area in (a), showing clustering of fine, acicular M_2C precipitates at lath boundaries and within the matrix (×8.8k); (**g**) CGHAZ after tempering for 4000 hours showing coarsened grain-boundary carbides and decreased matrix carbide density (×5.0k); and, (**h**) Enlargement of area in (g), showing coarsened acicular M_2C carbides in the matrix (×8.8k)

previously,[28,29] and it is possible that the segregation of impurity elements, particularly phosphorus, contributed to the decreased toughness through embrittlement of the grain boundaries and the grain-boundary/carbide interfaces.[17,23,28]

The impact toughness of the martensitic temper-bead HAZ has been shown to decrease as a result of the development of coarse grain-boundary carbides and it is known that martensitic 2.25Cr-1Mo steel exhibits poor creep resistance relative to bainitic and ferritic microstructures due to the rapid aging of fine carbides.[24,25] Dilatometer simulations of the thermal history of the temper-bead procedure have shown that martensite may form in 2.25Cr-1Mo steel over a wide range of heat inputs.[5]

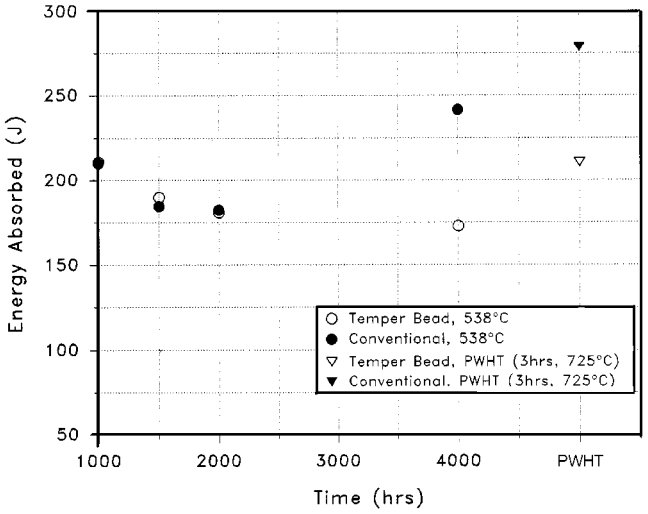

Fig. 11 Room-temperature impact toughness of the conventional weaving HAZ and the temper-bead HAZ as a function of tempering time and PWHT[15]

Hence, the temper-bead procedure may not be a suitable welding method for use with a 2.25Cr-1Mo steel.

4. Conclusions

- For the temper-bead welding procedure, the maximum as-welded hardness occurred within the CGHAZ and was approximately 400 HV. Overall, the conventional weaving procedure resulted in a softer as-welded HAZ than the temper-bead procedure. The maximum hardness of the bainitic CGHAZ was about 305 HV. For both of the welding procedures, the hardness decreased most rapidly within the first 100 h of tempering and was attributed to the precipitation of fine acicular M_2C. Subsequently, the rate of softening slowed drastically as hardness reduction was retarded by the slow coarsening rate of M_2C.
- The PWHT resulted in the most significant decrease in hardness. The maximum hardness within the PWHT CGHAZ of the conventional weaving HAZ was about 250 HV and that of the temper-bead HAZ was about 225 HV. Also, PWHT overaged the HAZ, causing the carbides to coarsen rapidly and a small amount of fine M_2C was retained. This could lower the creep resistance of the HAZ relative to the surrounding base metal and the weld metal, leading to localized creep deformation and accelerated creep rupture. The hardness of the HAZ tempered at the simulated service temperature of 538 °C approached the values achieved by PWHT between 1000 and 4000 h. A high density of M_2C was retained, which implies that the creep resistance of the HAZ will not be severely degraded relative to the surrounding material.

Acknowledgments

The authors would like to thank the University Research Incentive Fund (URIF) for their support of this research.

References

1. J. Orr, F.R. Beckitt, and G.D. Fawkes: *Ferritic Steels for Fast Reactor Steam Generators*, BNES, London, 1978, pp. 91-109.
2. R.F. Hoare: ERP/PMRL 81-75(TR), Canada Centre of Mineral and Energy Technology, Physical Metallurgy Research Laboratories, Ottawa, Canada, 1981.
3. G.S. Kim, J.E. Indacochea, and T.D. Spry: *J. Mater. Eng.*, 1988, vol. 10, pp. 117-32.
4. C.D. Buscemi, B.L. Jack, J.W. Skogsberg, and W.E. Erwin: *J. Eng. Mater. Technol.*, 1991, vol. 113, pp. 329-35.
5. J.T. Bowker, J.T. McGrath, R.F. Orr, M.W. Letts, and T.W. Lau: IIW Doc. IX. 1633.91CANMET, Ottawa, Canada.
6. T. Gladman and D. Dulieu: *Met. Sci.*, 1974, pp. 167-75.
7. K. Easterling: in *Introduction to the Physical Metallurgy of Welding*, Butterworth and Co., London, 1983, pp. 104-53.
8. M.F. Ashby and K.E. Easterling: *Acta Metall.*, 1982, vol. 30, pp. 1969-78.
9. R. Viswanathan: *Damage Mechanisms and Life Assessment of High-Temperature Components*, ASM International, Materials Park, OH, 1989, p. 208.
10. T.W. Lau and D. Hartwick: Report No. M90-33-K, Ontario Hydro Research Division, Toronto, Canada, 1990.
11. T.W. Lau and D. Hartwick: Report No. M91-61-K, Ontario Hydro Research Division, Toronto, Canada, 1991.
12. A.S. Oddy and R.S. Chandel: MTL 90-42(TR), CANMET, Ottawa, Canada.
13. E. Smith, B.E. Blanchard, and R.L. Apps: *Proc. Welding of Creep Resistant Steels Conf.*, TWI, 1970, pp. 79-89.
14. ASME Boiler and Pressure Vessel Code, Section I—Power Boilers, 1989 edition.
15. H. Baas: Master's Thesis, Queen's University, Kingston, ON, Canada, 1992.
16. *Metals Handbook*, ASM, Materials Park, OH, 1985, vol. 8, p. 90.
17. C.A. Hippsley: *Met. Sci.*, 1981, vol. 15, pp. 137-47.
18. J. Pilling and N. Ridley: *Metall. Trans. A*, 1982, vol. 13A, pp. 557-63.
19. C. Lundin and K. Khan: Progress Report, WRC, New York, NY, 1992.
20. C. Lundin, D. Yang, and K. Khan: Report of Research, WRC, New York, NY, 1987.
21. J.A. Todd: *Scripta Metall.*, 1986, vol. 20, pp. 269-74.
22. J. Janovec, A. Vyrostkova, and M. Svoboda: *Metall. Mater. Trans. A*, 1994, vol. 25A, pp. 267-75.
23. P. Doig, D. Lonsdale, and P.E.J. Flewitt: *Met. Sci.*, 1982, vol. 16, pp. 335-44.
24. K.J. Irvine and F.B. Pickering: *J. Iron Steel Inst.*, 1960, vol. 194, pp. 137-53.
25. R.G. Baker and J. Nutting: *J. Iron Steel Inst.*, 1959, vol. 193, pp. 257-68.
26. M.C. Murphy and G.D. Branch: *J. Iron Steel Inst.*, 1971, vol. 209, pp. 546-61.
27. J.H. Woodhead and A.G. Quarrell: *J. Iron Steel Inst.*, 1965, vol. 203, pp. 605-20.
28. P.K. Liaw, M.G. Burke, A. Saxena, and J.D. Landes: *Metall. Trans. A*, 1991, vol. 22A, pp. 445-68.
29. D.A. Curry and J.F. Knott: *Met. Sci.*, 1976, vol. 10, pp. 1-6.